



WEDNESDAY SLIDE CONFERENCE 2024-2025

Conference #21

26 March 2025

CASE I:

Signalment:

9-month-old female Sprague Dawley rat (*Rattus norvegicus*), SRG genotype (Rag2 & IL-2R γ knockout)

History:

This rat was part of a cancer implantation study using a novel cell line. Cancer cells were implanted around 3-months-old but failed to grow. The rat was monitored for delayed growth for an additional 6 months until its presentation to clinical staff. Weekly monitoring of this rat identified a drop in weight which persisted over a 3 week span despite clinical interventions, and the rat was ultimately euthanized.

Gross Pathology:

The urinary bladder was markedly distended by large amounts of red-tinged fluid, with blood-clots both suspended and adherent to the mucosal surface. The mucosal surface was red and roughened. Transmurally the bladder wall was red to black, and this change extended distally through the trigone and throughout the length of the urethra. At the distal end of the urethra, just proximal to the external genitalia were two large (3-5mm diameter), round, smooth, hard calculi (stones) occluding the lumen of the urethra. The stones were embedded within the mucosa and did not excise easily. Both ureters were distended with fluid (hydroureter). Both kidneys were moderately pale tan and had



Figure 1-1. Urinary bladder, rat. The urinary bladder was markedly distended by large amounts of red-tinged fluid. (Photo courtesy of: University of Michigan, Unit for Laboratory Animal Medicine, Pathology Core, <https://animalcare.umich.edu/business-services/ulam-pathology-core/>)

mildly bosselated subcapsular surfaces. There was mild to moderate dilation of the renal pelvis of both kidneys (hydronephrosis). From the renal pelvis, extending proximally through the renal papilla, medulla, and cortex is an irregular, friable, focal region of pallor.



Figure 1-2. Urinary bladder, rat. Two 3-5mm diameter, calculi are embedded in the urethral mucosa and occlude the lumen. (Photo courtesy of: University of Michigan, Unit for Laboratory Animal Medicine, Pathology Core, <https://animalcare.umich.edu/business-services/ulam-pathology-core/>)

Laboratory Results:

Bacteria Culture & Sensitivity: Tissue (kidney)

- *Staphylococcus xylosus* - Numerous
- *Enterobacter cloacae* complex - Few

Pneumocystis spp. Polymerase chain reaction (PCR): Tissue (lung)

- Negative

Microscopic Description:

Cytology (DifQuick):

Urine – Cytological preps of urine collected during necropsy showed large numbers of viable and degenerate neutrophils, streaming cellular debris, large numbers of bacterial cocci, and crystals. Bacteria are occasionally observed within neutrophils. Crystals are colorless and rhomboid (presumed struvite).

Histology (H&E):

Kidney - Extending from the renal pelvis into the medulla is a regionally extensive area of necrosis and marked suppurative inflamma-

tion with large numbers of cocci bacteria admixed throughout the cellular debris and neutrophils (pyelonephritis). The renal parenchyma in the vicinity of this lesion is characterized by interstitial edema, tubular degeneration and necrosis, with tubule lumina often containing eosinophilic proteinaceous fluid, neutrophils, cellular debris, and clusters of bacteria.

In addition to the pyelonephritis described above, there is mild bosselation of the capsular surface of the renal cortex. The cortical and medullary interstitium is expanded by extensive fibrosis with low numbers of mixed mononuclear inflammatory cells. Interstitial fibrosis often replaces tubular profiles. Remaining tubules frequently have markedly dilated lumens which range from empty to variably filled with eosinophilic proteinaceous fluid, fibrillar hyaline casts, or deeply basophilic granular material (mineralization). Tubular epithelial cells range from flattened /

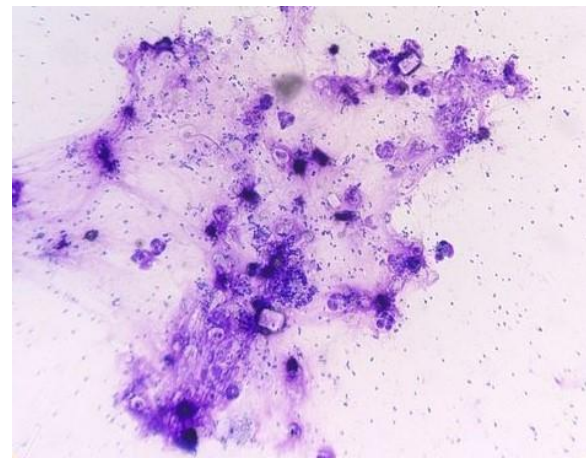


Figure 1-3. Urinary bladder, rat. Urine cytology shows large numbers of viable and degenerate neutrophils, streaming cellular debris, large numbers of bacterial cocci, and crystals. Crystals are colorless and rhomboid (presumed struvite) (Photo courtesy of: University of Michigan, Unit for Laboratory Animal Medicine, Pathology Core, <https://animalcare.umich.edu/business-services/ulam-pathology-core/>)

attenuated (atrophy) to swollen and vacuolated (degeneration) or are brightly eosinophilic, faded (lysis), and/or sloughed (necrosis). Glomeruli are frequently affected by one or more of the following changes: Dilation of the urinary space, marked global fibrosis of glomerular tufts (glomerulosclerosis), obsolescence of glomerular tufts, adherence of tufts to Bowman’s capsule (synechiae), thickening of Bowman’s capsule basement membrane.

Contributor’s Morphologic Diagnosis:

1. Kidney: Pyelonephritis, severe, acute, necro-suppurative, with intralesional cocci bacteria (Gram positive)
2. Kidney: Nephropathy, chronic, severe, with multifocal global glomerulosclerosis, periglomerular to interstitial fibrosis, tubular degeneration/necrosis with ectasia and proteinosis, and mild interstitial lymphohistiocytic nephritis (Chronic Progressive Nephropathy)



Figure 1-4. Urinary bladder, rat. There is an area of necrosis extending from the renal pelvis to the cortex. (Photo courtesy of: University of Michigan, Unit for Laboratory Animal Medicine, Pathology Core, <https://animal-care.umich.edu/business-services/ulam-pathology-core/>)

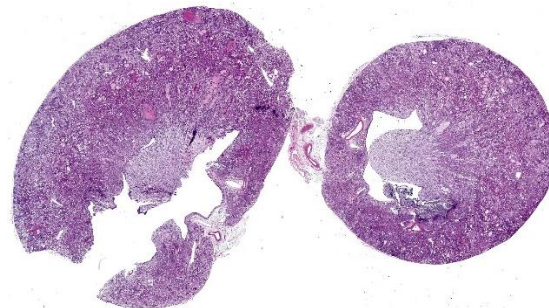


Figure 1-5. Urinary bladder, rat. Two sections of kidney are submitted for examination. Subgross lesions include tubular ectasia and interstitial fibrosis characteristic of chronic progressive nephropathy. The renal pelvis is mildly dilated and contains abundant cellular infiltrate. (HE, 8X)

Contributor’s Comment:

This case highlights the importance of using a range of diagnostic techniques—including cytology, special stains, and culture—alongside standard necropsy and histology to fully understand pathological processes. It serves as a valuable reminder to students to utilize all available tools rather than relying too heavily on one method. The gross identification of pyelonephritis and uroliths led to cytological identification of crystalluria consistent with struvite (triple phosphate/magnesium phosphate) crystals, which suggests the presence of urease producing bacteria. Common urease-producing bacteria associated with struvite crystalluria include: *Proteus* spp. (gram-negative bacillus), *Klebsiella* spp. (gram-negative bacillus), *Mycoplasma* spp. (gram-equivocal, pleomorphic), *Corynebacterium urealyticum* (gram-positive bacillus), and *Staphylococcus* spp. (gram-positive cocci). Histological evaluation and Gram staining highlighted clusters of gram-positive cocci, suggesting *Staphylococcus* spp. as the most likely agent from our differential list of urease-producing bacteria. Lastly, bacterial

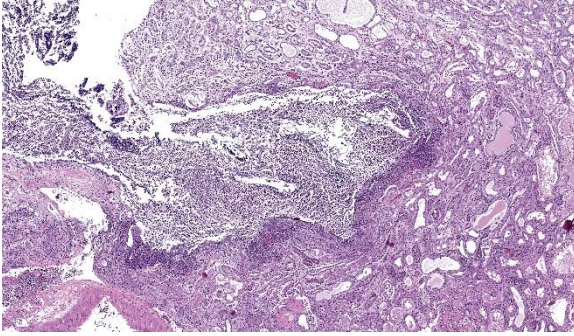


Figure 1-6. Urinary bladder, rat. There is necrosis of the renal papilla with extension into the overlying cortex. (HE, 88X)

cultures confirmed *Staphylococcus* (specifically *S. xylosus*) as the gram-positive cocci bacteria observed.

In laboratory mice and rats, pyelonephritis is most commonly caused by ascending infections from commensal or gastrointestinal bacteria.³ Urolithiasis is generally considered uncommon, but in cases of pyelonephritis becomes more common when the bacterial culprit is one of those mentioned previously (urease-producing). *Staphylococcus xylosus*, isolated in this case, is both a common commensal organism of rodents and is urease-producing.^{3,5,7}

Opportunistic infections from commensal organisms such as *S. xylosus* are likely exacerbated by immunodeficiencies/modulation. In the case of laboratory animals, cystitis and urolithiasis related to *S. xylosus* has been described in nude mice⁷ and severe dermatitis has been described in Rag2 / IL-2R γ knockout strains of mice¹ which are the same genes knocked out in the SRG strain rat utilized in this study.

The second morphological diagnosis proposed in this case is consistent with Chronic Progressive Nephropathy (CPN). This condition is one of the most well-described lesions

in laboratory rats.^{3,5} In particular, CPN is exceptionally common in Sprague-Dawley and Fischer 344 strains, with many rats developing clinically significant changes by 8-10 months old, and some developing histologic changes as early as 2-3 months.⁵ While CPN is generally thought of as a spontaneous or age related disease, it has been recognized that high-protein diets worsen the disease severity.^{3,5} Despite some persistent ambiguities in the pathogenesis of the condition, any resident or pathologist working in laboratory settings quickly becomes familiar with CPN and the spectrum of lesions it presents with, making it both a “classic” lesion as well as a practically relevant one.

Contributing Institution:

University of Michigan, Unit for Laboratory Animal Medicine, Pathology Core

<https://animalcare.umich.edu/business-services/ulam-pathology-core/>

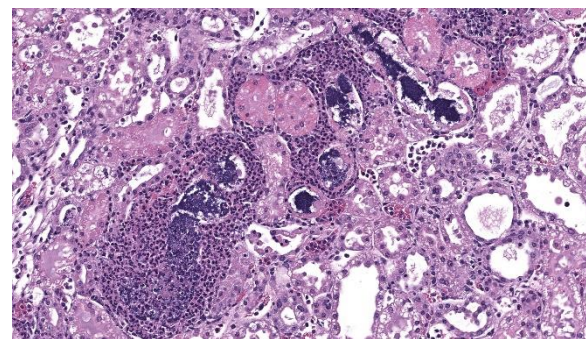


Figure 1-7. Urinary bladder, rat. Neutrophils and bacterial colonies ascend along renal tubules. (HE, 88X)

JPC Diagnosis:

1. Kidney: Tubular degeneration, necrosis, and regeneration, diffuse, moderate, with chronic interstitial lymphoplasmacytic nephritis.
2. Kidney: Pyelonephritis, necrotizing and suppurative, subacute, multifocal to coalescing, marked, with intratubular cocci, and mild hydronephrosis.

JPC Comment:

This week's moderator was Dr. Enrico Radaelli from the University of Pennsylvania's Comparative Pathology Core who led conference participants through a laboratory animal-centric conference with a few surprises. This first case is a succinct presentation with gross images and cytology that reinforce key slide interpretation. In particular, the history of urolithiasis and hydronephrosis is helpful in appreciating the irregular shape of the renal pelvis (especially in longitudinal section) and regional papillary necrosis which are discernable from the gross image. Gram-positive cocci are also numerous and consistent with the immunosuppressed state of this animal. We felt that pyelonephritis was the primary lesion in this case overall.

There was healthy debate among the group on our morphologic diagnosis. As the contributor notes, CPN is a common background lesion that inevitably encompasses changes at all levels of the nephron. We agree that these changes are present in this rat, though the severity was moderate for us compared with other conference cases we have reviewed (see Conference 23, Case 3, WSC 2012-2013 among others). We ran a Masson's trichrome stain which highlighted the multifocal and irregular distribution of fibrosis which aligns with the limited degree of capsular/contour change in this case as well. The rat in this

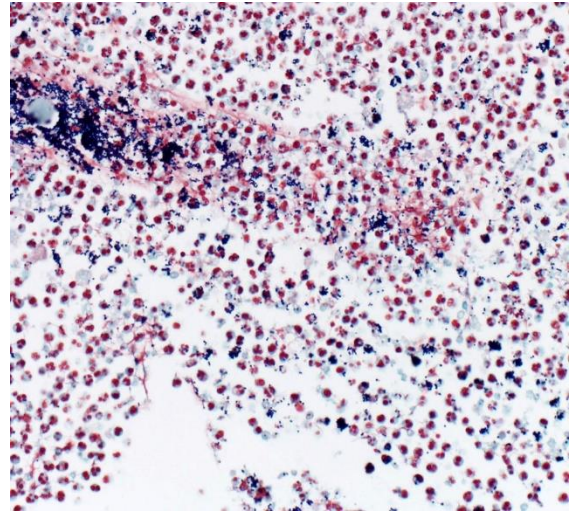


Figure 1-8. Urinary bladder, rat. A Gram stain demonstrates numerous gram-positive cocci within the renal pelvis. (Photo courtesy of: University of Michigan, Unit for Laboratory Animal Medicine, Pathology Core, <https://animalcare.umich.edu/business-services/ulam-pathology-core/>)

case was only nine months old at the time of euthanasia – for a comparison of CPN in a 2-year-old (24 months) rat and additional background literature, see Conference 12, Case 3, WSC 2019-2020.

Finally, Rag2 and IL-2R γ warrant a brief discussion of their role in immunity. The common gamma chain (IL-2R γ ; γ_c) of the IL-2 receptor is a conserved and important component in intracellular signaling for multiple cytokines, including IL-2, IL-4, IL-7, IL-9, and IL-21.^{2,4} Once ligands are bound to these receptors, γ_c forms a heterodimer and recruits Janus kinase 3 (JAK3) to further propagate these signals via STAT and induce changes in gene expression. These cytokines are vital for mature lymphoid cell proliferation (IL-2), T-helper type 2 responses (IL-4), early lymphoid/hematopoietic progenitor cell development (IL-7, IL-9), and natural killer cell development (IL-15, IL-21).^{2,4} As such, knock-out or mutation of IL-2R γ (such as in X-

linked SCID) results in significant impairment of NK, T-, and B-cells.⁶ Conversely, Rag2 forms one half (with RAG1) of a V(D)J recombinase that is essential for recombination of immunoglobulin and T-cell receptor variable regions that are needed for development of functional T- and B-lymphocytes.⁶ Defects in Rag2 are also associated with marked immunodeficiency. The combination of Rag2 and IL-2R γ defects is a substantial and additive deficit of both innate and adaptive immunity.

References:

1. Acuff NV, LaGatta M, Nagy T, Watford WT. Severe Dermatitis Associated with Spontaneous Staphylococcus xylosus Infection in Rag-/-T β 12-/- Mice. *Comp Med.* 2017 Aug 1;67(4):344-349.
2. Felsburg PJ, Hartnett BJ, Henthorn PS, Moore PF, Krakowka S, Ochs HD. Canine X-linked severe combined immunodeficiency. *Vet Immunol Immunopathol.* 1999 Aug 2;69(2-4):127-35.
3. Frazier KS, Seely JC, Hard GC, Betton G, Burnett R, Nakatsuji S, et al. Proliferative and Nonproliferative Lesions of the Rat and Mouse Urinary System. *Toxicologic Pathology.* 2012;40-86S.
4. Noguchi M, Yi H, Rosenblatt HM, Filipovich AH, Adelstein S, Modi WS, McBride OW, Leonard WJ. Interleukin-2 receptor gamma chain mutation results in X-linked severe combined immunodeficiency in humans. *Cell.* 1993 Apr 9;73(1):147-57.
5. Percy DH, Barthold SW, eds. *Pathology of Laboratory Rodents and Rabbits.* 4th ed. Blackwell Publishing; 2016:66.
6. Perryman LE. Molecular pathology of severe combined immunodeficiency in mice, horses, and dogs. *Vet Pathol.* 2004 Mar;41(2):95-100.
7. Salleng KJ, Jones CP, Boyd KL, Hicks

DJ, Williams MM, Cook RS. Staphylococcus xylosus Cystitis and Struvite Urolithiasis in Nude Mice Implanted with Sustained-release Estrogen Pellets. *Comp Med.* 2018;68(4):256-60.

CASE II:

Signalment:

An adult female Sprague Dawley rat (*Rattus norvegicus*)

History:

Patient presented with a multilobulated, firm facial mass on the left maxilla. Fine needle aspirate not consistent with abscessation or inflammation.

Gross Pathology:

The subcutis at the base of the left pinna is expanded by a firm, bilobed mass. The upper lobe is spherical and measures 2 cm along the widest axis; the lower lobe is spherical and measures 1 cm along the widest axis. On cut surface, the mass is well circumscribed, has a fibrous capsule, and centrally contains copious amounts of friable, tan to pink material. The central material often displays a laminar appearance.

Microscopic Description:

Haired skin: Examined are two sections of haired skin containing the grossly reported mass, skeletal muscle, and dermal adnexa. The mass is an expansile, well demarcated, and variable cellular neoplasm composed of well differentiated squamous epithelium arranged in trabeculae, islands, and papillary projections supported by pre-existing fibrovascular stroma. The neoplastic cells often exhibit sebaceous differentiation, with the

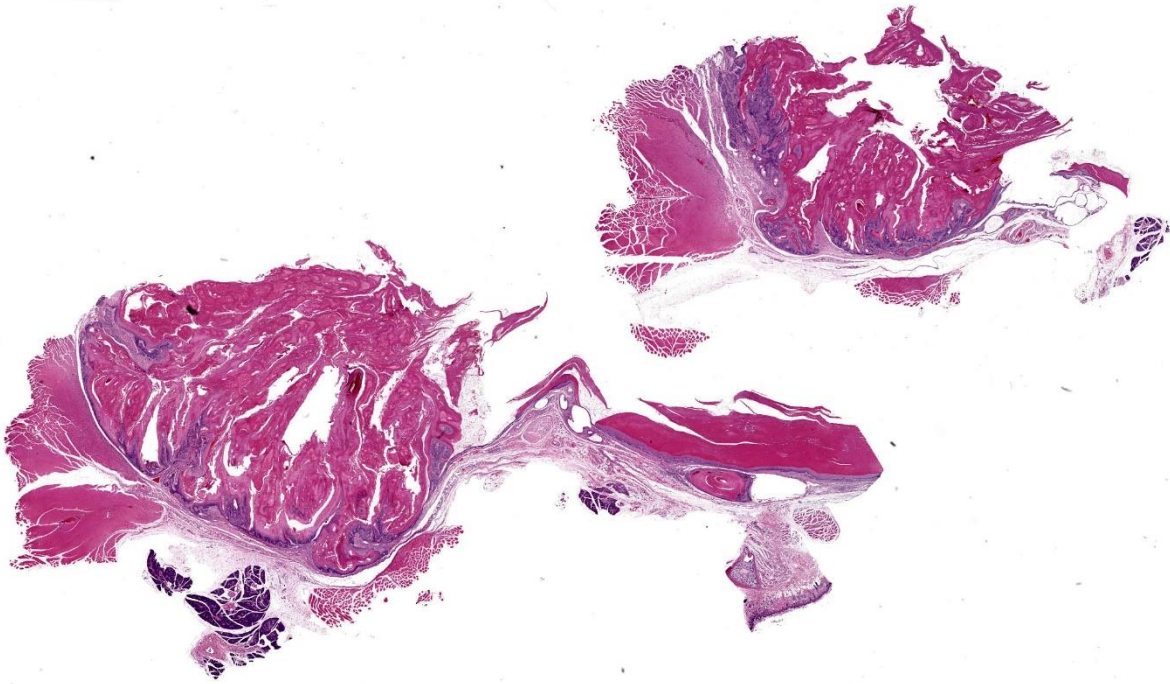


Figure 2-1. Zymbal's gland, rat. Two sections of Zymbal's gland are submitted for examination. There is marked proliferation of the squamous epithelium with large lamellae of keratin extending into the lumen.

mass centrally displaying squamous differentiation leading to abrupt keratinization organized into lamellated keratin and keratin pearls. The neoplastic cells have distinct cell borders, moderate to abundant finely vacuolated, eosinophilic cytoplasm, and round to ovoid nuclei containing finely stippled chromatin with one to two prominent nucleoli. Anisokaryosis and anisokaryosis are mild. Nine mitotic figures are observed in 10 HPF (2.37mm²). Few aggregates of lymphocytes, plasma cells, eosinophils, and neutrophils infiltrate the dermis adjacent to the mass. Apocrine glands adjacent to the mass are moderately dilated and contain scant, pale eosinophilic, acellular material.

Contributor's Morphologic Diagnosis:
Zymbal's gland: Adenoma

Contributor's Comment:

Histologic evaluation of the mass is consistent with a Zymbal's gland tumor due to cellular morphology (specifically sebaceous differentiation of neoplastic cells) and anatomic location. An adenoma is diagnosed based on the lack of invasion into the underlying stroma. Zymbal's gland adenomas arise from Zymbal's holocrine glands at the base of the external ear.^{1,2} These tumors often exhibit vacuolated cytoplasm, well differentiated squamous epithelium, and robust keratinization which are features in this case as well.^{1,2}

Differentiation between an adenoma and a carcinoma of the Zymbal's gland can be achieved based on histomorphology and growth patterns.¹ Diagnostic features associ-

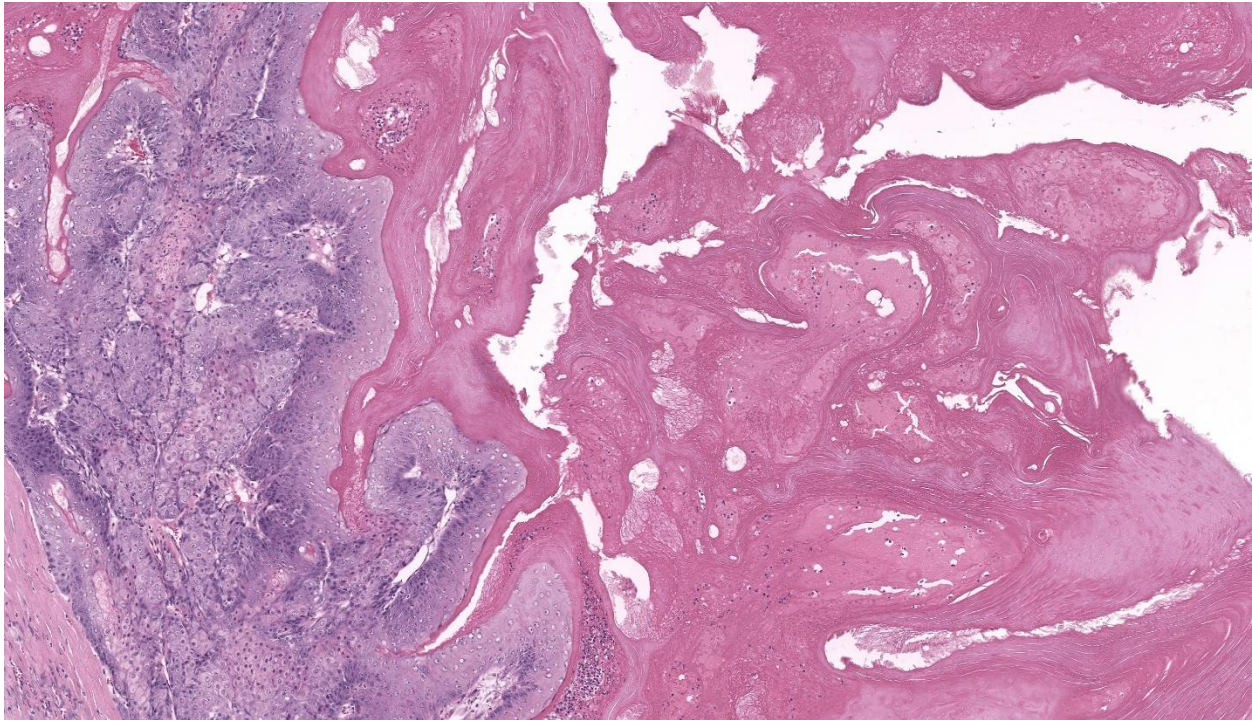


Figure 2-2. Zymbal's gland, rat. Higher magnification of the wall of the tumor with proliferating sebocytes, and more centripetally, proliferating squamous epithelium with layers of lamellated keratin and ghost cells.

ated with adenomas include well-differentiated neoplastic cells, lobulated structure, a mixture of both basaloid and mature sebaceous cells, cystic areas, and lack of nuclear atypia.² Diagnostic features associated with carcinomas include ulceration, irregular acini, papillary projections into cystic cavities, frequent mitoses, and increased cellular pleomorphism.² Differential diagnoses for an adenoma include glandular hyperplasia or a well-differentiated carcinoma while those for a carcinoma include an adenoma (for well-differentiated carcinomas) or squamous papilloma.²

Zymbal's glands are mostly observed and described in rats, however the structure is also present in mice.² Zymbal's gland typically measures approximately 3 to 5 mm in diameter, and is composed of three to four lobules.² While spontaneous tumors are uncommon, Zymbal's gland tumors are one of the most

common tumor types in chemical associated carcinogenesis studies in laboratory rodents.^{3,4,5} Specifically, Zymbal's gland tumors have been shown to be inducible by mutagenic compound 2-amino-3-methylimidazo[4,5-f]quinoline among other chemical mutagens.⁵

Contributing Institution:

North Carolina State University College of Veterinary Medicine Department of Population Health and Pathobiology

<https://cvm.ncsu.edu/php/>

JPC Diagnosis:

Zymbal's gland: Adenoma

JPC Comment:

This second case is a WSC classic with elements such as the parotid salivary gland, auricular cartilage, and cheek muscle aiding in tissue identification. Conference participants discussed differential diagnoses including papilloma and keratoacanthoma due to the abundant keratin in section. As the contributor notes, sebaceous differentiation of neoplastic cells is a key feature to distinguish a Zymbal's gland tumor. Likewise, serial sections of this neoplasm might appear widely different (more or less sebaceous cells present) given the heterogenous distribution of these cells. We agree with the contributor that this neoplasm is an adenoma given the lack of invasion and bland cellular features. We attribute the presence of mixed inflammatory cells and edema to the inflammatory stimulus of abundant keratin. Dr. Radaelli emphasized that Zymbal's gland tumors resemble clitoral and preputial gland neoplasms given the cell of origin, though the supporting architecture is different.²

References:

1. Percy DH, Barthold SW, eds. Pathology of Laboratory Rodents and Rabbits. 4th ed. Blackwell Publishing; 2016.
2. Rudmann D, Cardiff R, Chouinard L, et al. Proliferative and Nonproliferative Lesions of the Rat and Mouse Mammary, Zymbal's, Preputial, and Clitoral Glands. Toxicologic Pathology. 2012;40(6_suppl):7S-39S.
3. National Toxicology Program. Toxicology and Carcinogenesis Studies of 8-Methoxypsoralen (CAS No. 298-81-7) in F344/N Rats (Gavage Studies). Natl Toxicol Program Tech Rep Ser. 1989 Jul;359:1-130.
4. Pucheu-Haston CM, Brandão J, Jones KL, et al. Zymbal gland (auditory sebaceous gland) carcinoma presenting as otitis externa in a pet rat (*rattus norvegicus*).

Journal of Exotic Pet Medicine. 2016; 25(2):133–138.

5. Makino H, Ishizaka Y, Tsujimoto A, et al. Rat p53 gene mutations in primary Zymbal gland tumors induced by 2-amino-3-methylimidazo[4,5-f]quinoline, a food mutagen. Proc Natl Acad Sci U S A. 1992 Jun 1;89(11):4850-4.

CASE III:**Signalment:**

1-year-old male intact standard fancy rat (*Rattus norvegicus domestica*)

History:

Submitted for necropsy is the body of a 1-year-old male intact pet rat adopted from a rescue a few months prior, with a reported history of waxing and waning nodular facial swelling located under the right eye, followed by diffuse facial swelling. This progressed to upper respiratory signs that resolved with enrofloxacin. The facial swelling was treated with a course of prednisolone and meloxicam. After a period of treatment, the signs worsened, characterized by a new eruption of multiple firm nodules near the nasal angle of the eyes and over the snout with increased respiratory distress. After 48h of increased respiratory rate and effort along with difficulty swallowing, the patient was euthanized due to poor prognosis.

Gross Pathology:

The lungs are entirely replaced, severely deformed, and expanded by over three dozen variably sized, up to 3.8 x 2.4 x 1.8 cm, multifocal to coalescing spherical, tan masses, rendering a bosselated appearance to the parenchyma, in particular of the right lung. On cut section, the masses extend deep within the parenchyma and exude abundant thick, opaque, light-yellow to white, malodorous pasty material (suppurative pneumonia with

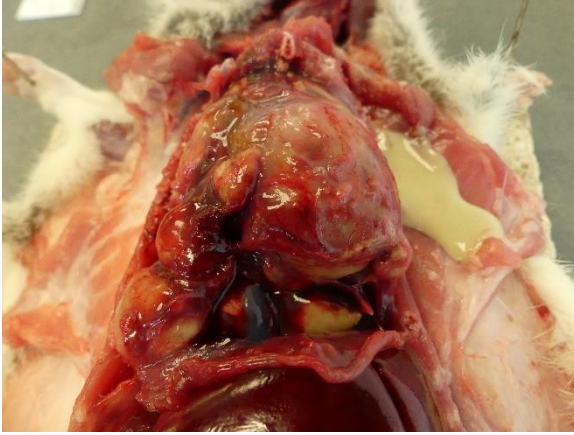


Figure 3-1. Lungs, rat. The lungs have a bosselated appearance, the right lung in particular. (Photo courtesy of: Cornell University College of Veterinary Medicine – Animal Health Diagnostic Center, Department of Biomedical Science, Section of Anatomic Pathology; <https://www.vet.cornell.edu/animal-health-diagnostic-center>)

bronchiectasis). Additionally, the pleura firmly adheres multifocally to the diaphragm and thoracic wall, and the heart is obscured by a pale pink mass of suppurative material and fibrosis (pericardial abscess).

Laboratory Results:

Bacterial culture was performed of the lungs, which isolated both *Mycoplasma sp.* and *Rodentibacter pneumotropicus*. Further speciation of *Mycoplasma sp.* was not conducted. Exclusion of *Filobacterium rodentium* was initially desired; unfortunately, the specific type of culture medium for this agent was not available at the testing facility.

Microscopic Description:

Lung: Up to 85% of the parenchyma in the submitted sections is effaced and replaced by variable numbers of well-delineated, coalescing spherical nodules arising within severely ectatic pre-existing bronchi (bronchiectasis),

and enclosed in a thick fibrous capsule stippled with admixed lymphocytes, plasma cells, and macrophages, along with scattered stout congested capillaries. These nodules are mostly composed of central, compact amorphous eosinophilic material, vaguely imprinted with leukocytic debris, and rimmed by abundant degenerate neutrophils. The bronchial epithelium lining the areas of bronchiectasis is circumferentially replaced by an up to 10 cells-thick, keratinizing stratified squamous epithelium (squamous metaplasia). Covering this epithelium and projecting towards the lumen are mats of up to 18.0µm-long and 1.0µm thick, faintly amphophilic to eosinophilic filamentous bacteria.

Remnant alveoli within the surrounding parenchyma are compressed, distorted and completely filled with degenerate neutrophils, lymphocytes, plasma cells and foamy macrophages, embedded within variable quantities of light eosinophilic, proteinaceous fluid (pulmonary edema). The alveolar lining is extensively replaced by a continuous single cell-thick, low-cuboidal epithelium (pneumocytes type II hyperplasia). When appreciable, bronchial glands are prominent, mildly distorted and hyperplastic. Variably throughout the sections, bronchioles and bronchi are severely cuffed by abundant admixed lymphocytes and plasma cells, equally encircling infrequently thrombosed pulmonary arterioles.

Two additional stains, modified Steiner and Gram, were applied to a section of lung. The modified Steiner highlighted a thick mat of up to 18.0 µm-long, free filamentous argyrophilic bacteria corresponding to the organisms appreciated on hematoxylin eosin, disposed perpendicularly to the metaplastic bronchial epithelium. Thousands of identical free bacteria were distributed throughout the suppurative material filling the ectatic bronchi.

The Gram stain highlighted similar Gram-negative, filamentous bacteria throughout the



Figure 3-2. Lungs, rat. The lungs are expanded by over three dozen tan masses ranging up to up to 4cm, multifocal to coalescing spherical, tan masses. (Photo courtesy of: Cornell University College of Veterinary Medicine – Animal Health Diagnostic Center, Department of Biomedical Science, Section of Anatomic Pathology; <https://www.vet.cornell.edu/animal-health-diagnostic-center>)

sections, covering the metaplastic bronchial epithelium and interspersed with sparsely scattered Gram-negative, 0.3 μm -long coccobacilli. Clusters of approximately 0.2 μm in diameter, Gram-positive coccobacilli were additionally dispersed throughout the suppurative material.

Contributor's Morphologic Diagnosis:

Lung: Severe, multifocal to coalescing, chronic suppurative bronchopneumonia with bronchiectasis and myriad intralesional filamentous bacteria, lymphoplasmacytic peribronchiolitis and perivascularitis, squamous metaplasia of airways epithelium, glandular hyperplasia, type II pneumocyte hyperplasia, thrombosis and edema

Contributor's Comment:

Grossly, this case was unusually extensive with regards to the diffuse bilateral involvement of the pulmonary parenchyma, although the lesions remained more severe within the right lung, consistent with the classic unilateral, cranio-ventral lesional distribution commonly encountered with *Mycoplasma pulmonis*.

Isolation of *Mycoplasma* sp. together with bronchiectasis allowed for a diagnosis of murine respiratory mycoplasmosis, also termed chronic respiratory disease (CRD). CRD is usually considered subsequent to the combined action of *Mycoplasma pulmonis* and other respiratory pathogens such as *Filobacterium rodentium* (formerly known as CAR bacillus),⁴ viral pathogens such as Sendai virus and rat coronavirus, and/or environmental causes such as high levels of ammonia.^{1,3}

Mycoplasma pulmonis is directly deleterious to the respiratory epithelium, and is considered the only clinically relevant species of *Mycoplasma* in rodents.^{1,3} Transmission occurs vertically or via aerosols, although the latter has experimentally proven fairly inefficient.^{1,8} Colonization of the respiratory tract by *Mycoplasma* sp. results in ciliostasis and loss of cilia, subsequently reducing the efficacy of the mucociliary escalator, and caus-



Figure 3-3. Lung, rat. Bronchioles are diffusely ectatic and filled with eosinophilic cellular exudate. Adjacent alveoli are compressed. (HE, 381X)

ing mucus and inflammatory exudate accumulation within the airways. Ultimately, the ongoing buildup of lysozyme-rich inflammatory material culminates in permanent damage and dilatation of airways, resulting in bronchiectasis.^{1,3} Both *Mycoplasma* microorganisms and host cell membrane fragments nonspecifically stimulate B-cell mitosis, and the resulting florid peribronchiolar lymphocytic infiltration is a salient histological feature of CRD in rats.¹ Other respiratory manifestations of mycoplasmosis in rats include rhinitis and lymphoplasmacytic tracheitis.^{1,8}

Given the tropism of *M. pulmonis* for ciliated epithelia, colonization and consequent inflammation of non-respiratory tissues, including the middle ear, endometrium and synovium, may also occur.^{1,3} *M. pulmonis* is usually not evident on hematoxylin eosin sections, and requires ancillary tests such as culture or PCR for confirmation.

Additionally in this rat, the myriad amphiphilic to light basophilic filamentous bacteria appreciated lining the inside of ectatic bronchi were considered compatible with *Filobacterium rodentium*, formerly known as Cilia-Associated Respiratory (CAR) bacillus.⁴ *F. rodentium* is mostly transmitted by close contact during the neonatal period, and most strains of laboratory rats have been shown uniformly susceptible to disease.^{1,3} While *M. pulmonis* and *F. rodentium* co-infection is frequent, both may individually cause illness and result in similar clinical disease and histological lesions.^{1,3,8}

Histologically, *F. rodentium* is best highlighted using silver stains (such as Warthin-Starry), and characteristically forms mats of filamentous bacteria colonizing the respiratory airways, interspersed with cilia and oriented in a relatively perpendicular fashion to the epithelium.¹ *F. rodentium* has been isolated from the respiratory epithelium of other

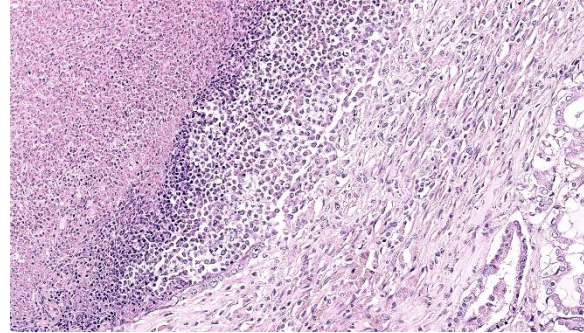


Figure 3-4. Lung, rat. Bronchiolar wall, with necrotic luminal exudate (left), a rim of viable neutrophils and fewer macrophages (center), and a fibrotic wall (right).

species than rat, including mice, rabbits, cattle, goats and pigs, and a recent report suggests that a particular strain of *Filobacterium sp.* could be associated with chronic bronchitis in cats.^{1,5}

In the present case, these argyrophilic bacteria were emphasized using modified Steiner's stain, which additionally revealed a significant number of those microorganisms within the suppurative material filling the airways. On Gram stain, the organisms appeared faintly Gram-negative. As mentioned in the above laboratory results section, confirmation by culture was unavailable as *F. rodentium* requires specific growth media,^{1,7} and this remains presumptive based on the combined histomorphological features, staining characteristics, and common reported co-involvement of *M. pulmonis* and *F. rodentium* in CRD.

Large numbers of *Rodentibacter pneumotropicus* were additionally isolated via lung culture. Formerly known as *Pasteurella pneumotropica*,² this Gram-negative, 0.5 to 1.2 μm -long rod to coccobacillus is a resident bacterium of the respiratory flora in rats,^{1,3} and was thus considered an opportunistic co-infectious agent in the present case. Although not isolated on culture, clusters of Gram-positive bacteria were histologically appreciated;

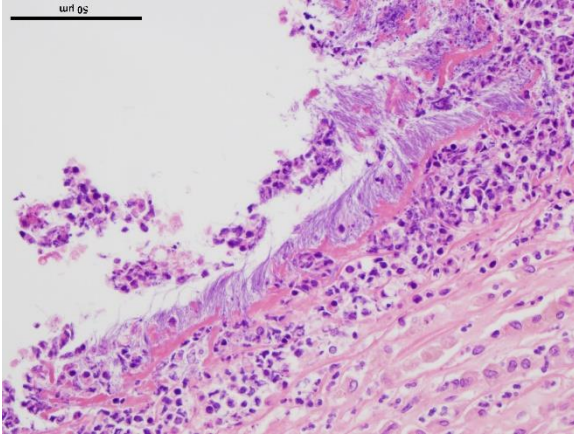


Figure 3-5. Lung, rat. Cilia are basophilic due to numerous intertwined filamentous bacilli. (Photo courtesy of: Cornell University College of Veterinary Medicine – Animal Health Diagnostic Center, Department of Biomedical Science, Section of Anatomic Pathology; <https://www.vet.cornell.edu/animal-health-diagnostic-center>) (HE, 400X)

Gram-positive organisms involved in respiratory disease and inducing formation of abscesses in rats include *Streptococcus pneumoniae* and *Corynebacterium kutscherii*, the latter capable of causing cutaneous abscesses.^{1,3}

Additional findings, not present in the submitted slides, include the presence of nematode parasites within the renal pelvis, considered consistent with *Trichosomoides crassicauda*, a roundworm that commonly invades the murine urinary tract in individuals housed in poor hygienic conditions.⁶ About five deep subcutaneous abscesses were additionally noted throughout the skin of the muzzle, with no identifiable intralesional bacteria. This was considered most probably consecutive to dissemination from the lungs in a relatively immunocompromised animal, given the absence of florid lymphoid hyperplasia in the present case, usually expected with *Mycoplasma sp.* infection.

Contributing Institution:

Cornell University College of Veterinary

Medicine – Animal Health Diagnostic Center, Department of Biomedical Science, Section of Anatomic Pathology

<https://www.vet.cornell.edu/animal-health-diagnostic-center>

JPC Diagnosis:

Lung: Bronchopneumonia, suppurative, chronic, diffuse, severe, with bronchiectasis, fibrosis, and cilia-associated bacilli and luminal colonies of coccobacilli.

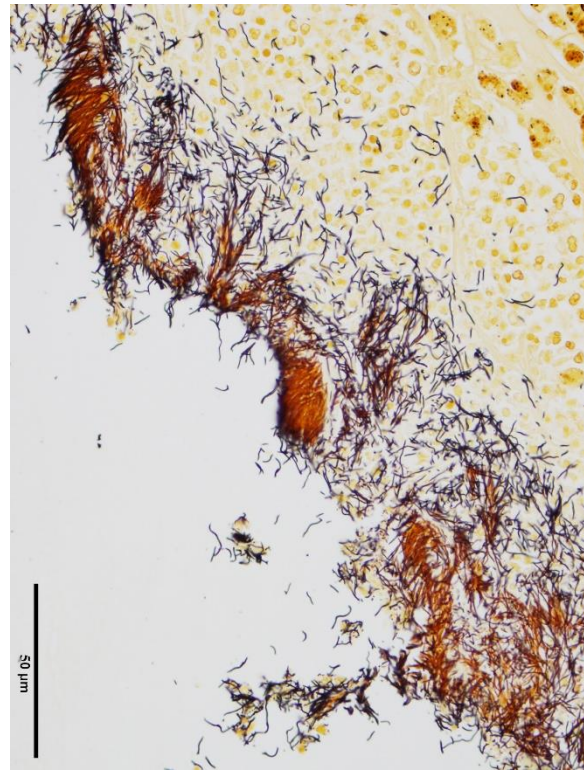


Figure 3-6. Lung, rats. A sliver stain demonstrates masts of filamentous bacilli within the cilia of the airway-epithelium. (Photo courtesy of: Cornell University College of Veterinary Medicine – Animal Health Diagnostic Center, Department of Biomedical Science, Section of Anatomic Pathology; <https://www.vet.cornell.edu/animal-health-diagnostic-center>) (Steiner's, 400X)

JPC Comment:

The third case of this conference has a terrific macroscopic-microscopic correlation.. We confirm the contributor's interpretation of abundant argyrophilic filamentous bacteria with both Warthin-Starry and methenamine silver highlighting organisms within ectatic bronchioles well. We also noted a mixed population of bacteria on our Gram stain consistent with secondary opportunistic infection following ciliostasis initiated by *Mycoplasma*. Although subtle, there is also a change in appearance of ciliated epithelium with replacement of the normal eosinophilic hue towards a basophilic appearance of the cilia. Although non-specific, this is corroborating evidence of 'something added' such as *Mycoplasma*, *Bordetella*, or *Filobacterium* and can be seen even in sloughed epithelium. Although not stated by the contributor, we suspect that this animal likely had concurrent *Mycoplasma* in the ear to explain the facial signs observed.

Conference participants also discussed the presence of "oat cells" (ruptured leukocytes with streaming nuclear contents) which were a significant feature of this case. Oat cells have been described secondary to leukotoxins, a type of repeats in toxin (RTX) which is an important virulence factor for several bacterial pathogens including *Mannheimia*, *Pasteurella*, and *Bordetella* among others.¹¹ Leukotoxins can enhance both recruitment and killing of leukocytes which confers an advantage in both hampering the host immune response and extracting cellular resources for future growth. *Rodentibacter pneumotropicus* (formerly *Pasteurella pneumotropica*) is a potential source of RTX toxin in this case,¹⁰ given the gram-negative coccobacilli we noted in section. Interestingly, lysis of leukocytes may be a double-edged sword, as extru-

sion of nuclear chromatin also enhances NETosis and may entrap and kill a portion of the bacteria concurrently.⁹

References:

1. Barthold SW, Griffey SM, Percy DH, eds. *Pathology of Laboratory Rodents and Rabbits*. 4th ed. Ames, IA: Wiley-Blackwell; 2016: 133-136, 140-141, 144-145.
2. Benga L, Sager M, Christensen H. From the [Pasteurella] pneumotropica complex to *Rodentibacter* spp.: an update on [Pasteurella] pneumotropica. *Vet. Microbiol.* 2018;217:121-134.
3. Fox JG, Anderson LC, Otto GM, Prtichett-Corning KR, Whary MT, eds. *Laboratory animal medicine*. 3rd ed. San Diego, CA: Elsevier; 2015:166-169, 173-175.
4. Ike F, Sakamoto M, Ohkuma M. et al. *Filobacterium rodentium* gen. nov., sp. nov., a member of Filobacteriaceae fam. nov. within the phylum Bacteroidetes; includes a microaerobic filamentous bacterium isolated from specimens from diseased rodent respiratory tracts *Int. J. Syst. Evol.* 2016; 66:150-157.
5. Načeradská M, Pekova S, Danesi P. et. A novel *Filobacterium* sp can cause chronic bronchitis in cats. *PLOS ONE*. 2021;16(6):e0251968.
6. Najafi F, Ghadikolai MT, Naddaf SR. et al. *Trichosomoides crassicauda* infection in laboratory rats with histopathological description in the bladder tissue. *J Med Microbiol Infec Dis.* 2017;5(1-2):31-34.
7. Nietfeld JC, Fickbohm BL, Rogers DG, Franklin CL, Riley LK. Isolation of cilia-associated respiratory (CAR) bacillus from pigs and calves and experimental infection of gnotobiotic pigs and rodents. *J. Vet. Diagn. Invest.* 1999;11:252-258.
8. Rothenburger JL, Himsworth CG,

Clifford CB, Ellis J, Treuting PM, Leighton FA. Respiratory Pathology and Pathogens in Wild Urban Rats (*Rattus norvegicus* and *Rattus rattus*). *Veterinary Pathology*. 2015;52(6):1210-1219.

9. Aulik NA, Hellenbrand KM, Klos H, Czuprynski CJ. *Mannheimia haemolytica* and its leukotoxin cause neutrophil extracellular trap formation by bovine neutrophils. *Infect Immun*. 2010 Nov;78(11):4454-66.
10. Sasaki H, Ueshiba H, Yanagisawa N, Itoh Y, Ishikawa H, Shigenaga A, Benga L, Ike F. Genomic and pathogenic characterization of RTX toxin producing *Rodentibacter* sp. that is closely related to *Rodentibacter haemolyticus*. *Infect Genet Evol*. 2022 Aug;102:105314.
11. Srikumaran S. Leukotoxins. *Toxins (Basel)*. 2020 Apr 7;12(4):231.

CASE IV:

Signalment:

9-week-old, female, human-peripheral blood mononuclear cell (huPBMC)-engrafted-NOD *scid* gamma (NSG) mouse (*Mus musculus*)

History:

Female, human peripheral blood mononuclear cell (hPBMC)-engrafted NOD *scid* gamma (NSG) mouse purchased from an approved vendor, was submitted from an experimental cohort of mice experiencing similar clinical course of disease. One week after arrival, this cohort underwent experimental injection of MDA-MB-231 human breast cancer cells into the subcutis of the left flank (tumor xenograft model). In the 2 weeks following injection, the cohort demonstrated significant weight loss (3-5g), poor tumor engraftment, and unexpectedly high mortality. This mouse was euthanized and submitted for

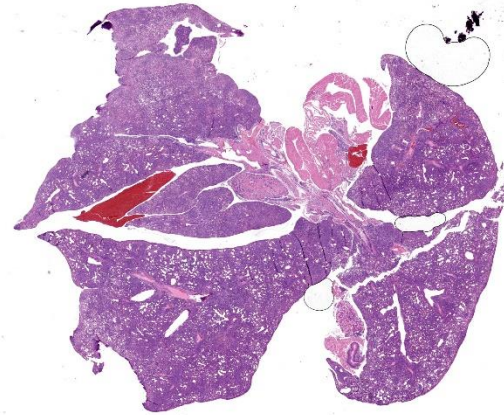


Figure 4-1. Lungs, scid mouse. There is diffuse atelectasis of the lungs. (HE, 6X)

post-mortem examination as a representative animal.

Gross Pathology:

The mouse weighed 16.15g and was in thin body condition (1.5/5 BCS); expected body weight for a female 9-week-old NSG mouse is 23.3 +/- 1.6g. There was diffuse pallor of the tail, ears and mucous membranes, and marked depletion of subcutaneous and visceral adipose. Scant white fascia-like tissue was noted at the tumor injection site, without evident tumor growth. The liver weighed 0.99 g (6.1% BW), was tan, and had rounded edges and a subtly irregular surface.

Microscopic Description:

All lung lobes demonstrate multifocal to coalescing consolidation and atelectasis with interstitial and alveolar septal thickening by mononuclear inflammatory cells and plump spindle cells (fibroplasia). Alveoli are multifocally lined by a continuous layer of plump, cuboidal to polygonal, epithelial cells (type II pneumocyte hyperplasia). There are dense perivascular and peribronchiolar lymphocytic cuffs up to 15 cells thick that contain low to moderate numbers of mitotic figures and

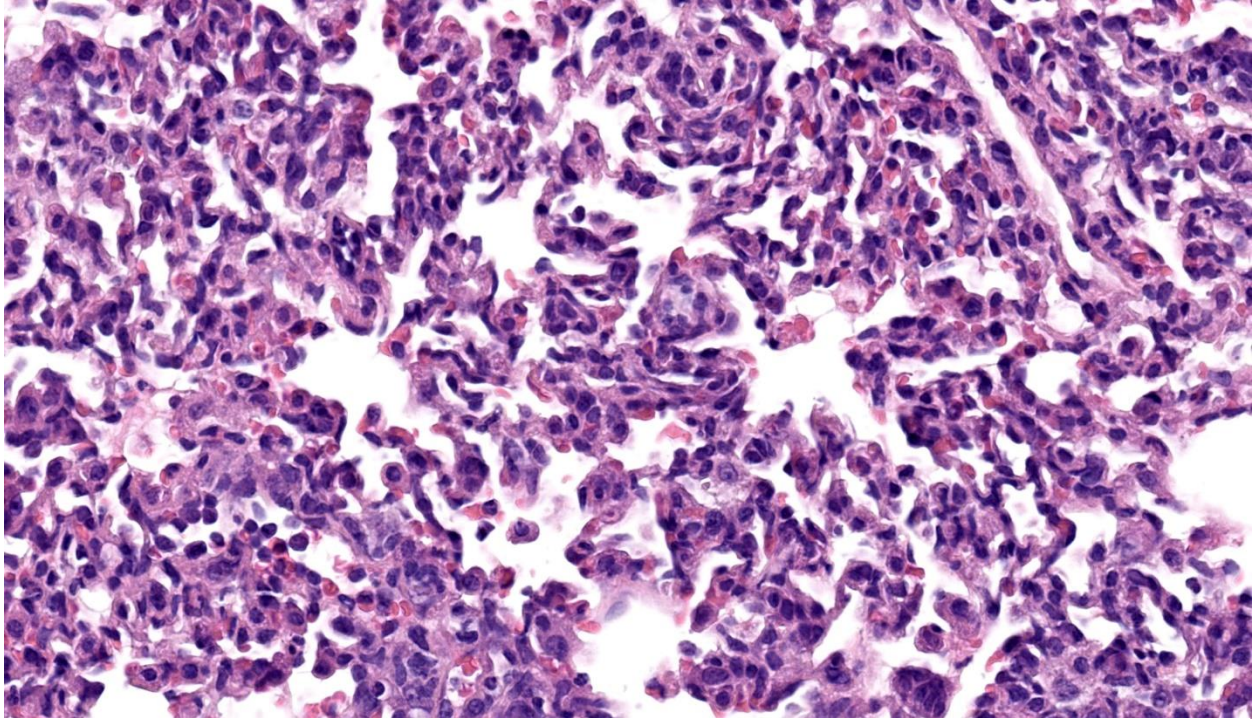


Figure 4-2. Lung, scid mouse. Diffusely, alveolar septa are hypercellular and expanded by hypertrophy of septal macrophages, circulating neutrophils, mild edema, and type II pneumocyte hyperplasia. (HE, 733X)

apoptotic bodies. Lymphocyte nuclei are subjectively slightly larger than expected (in mice).

Esophageal mucosa has multifocal vacuolar degeneration and scattered apoptosis involving basal epithelial cells, and an underlying cell-rich band of lymphocytic inflammation with fewer macrophages and scattered neutrophils along the basement membrane interface. Lymphocytic and neutrophilic inflammation extends transmurally, with severe mononuclear infiltration and aggregation in the tunica muscularis. Associated changes in skeletal muscle fibers include: 1) rounded myofibers with pale sarcoplasm lacking cross-striations and internalization of nuclei (degeneration), 2) shrunken and rounded myofibers with small hyperchromatic nuclei (atrophy), or 3) effacement and replacement of myofibers by lymphocytic inflammation (myofiber loss).

Immunohistochemistry:

Immunohistochemistry confirmed that perivascular and peribronchiolar cuffs in the lung and interface inflammation in the esophagus are primarily CD3+ cells (consistent with T lymphocytes), with low to moderate numbers of Iba-1+ leukocytes (interpreted as macrophages).

Contributor's Morphologic Diagnosis:

Lung:

Inflammation, perivascular to peribronchiolar to interstitial, lymphoproliferative and histiocytic, chronic and active, severe, with interstitial lung injury, chronic atelectasis, and type II pneumocyte hyperplasia

Esophagus:

Mucosa, basal epithelial cell vacuolization and apoptosis

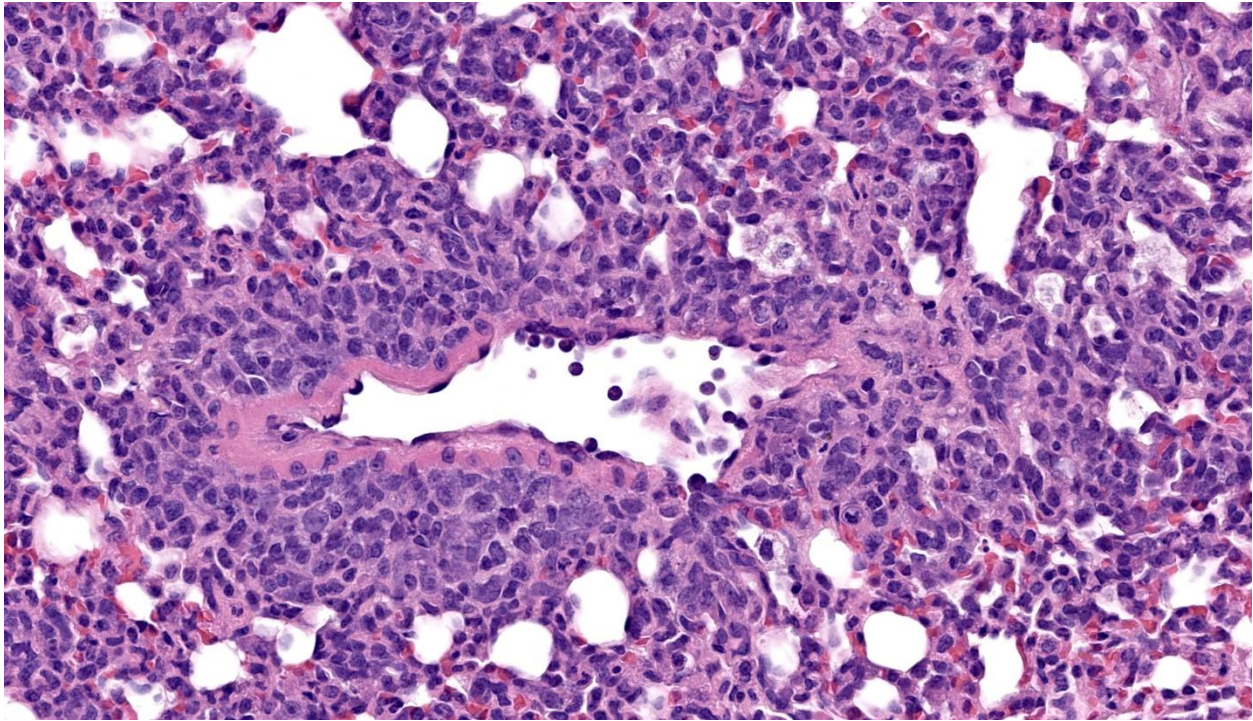


Figure 4-3. Lung, scid mouse. There are cuffs of large lymphocytes and histiocytes around blood vessels throughout all lung lobes. (HE, 733X)

Esophagitis, ‘interface’, lymphocytic with fewer neutrophils and macrophages, multifocal to coalescing, severe, with marked submucosal and muscularis lymphocytic infiltration, and myofiber degeneration, atrophy and loss.

Condition:

Xenogeneic Graft versus Host Disease (GvHD)

Contributor’s Comment:

Dense multiorgan infiltration by large lymphocytes with associated epithelial degeneration/apoptosis and a 1) a lichenoid interface pattern in skin, mucous membranes and esophagus, 2) a perivascular distribution in lung, salivary gland, and pancreas, and 3) a portal distribution in the liver are consistent

with Graft-versus-Host Disease (GvHD).^{10,11,14}

GvHD is a life-threatening, systemic inflammatory condition mediated by alloreactive transplanted donor lymphocytes that recognize antigenic disparities between donor (graft) and recipient (host) tissues leading to a cell-mediated adaptive immune response. The principle (but not exclusive) antigens driving GvHD are differences in Major Histocompatibility Complex (MHC) class I and II expression between donor and recipient tissues, as these molecules can be highly polymorphic between individuals.⁸ MHC class I molecules are expressed on the cell surface of all nucleated cells, whereas MHC class II expression is largely limited to antigen presenting cells such as macrophages, dendritic cells, and B lymphocytes. A major component of T cell maturation in the thymus is the process of central tolerance where immature, self-reactive T cells are removed to prevent

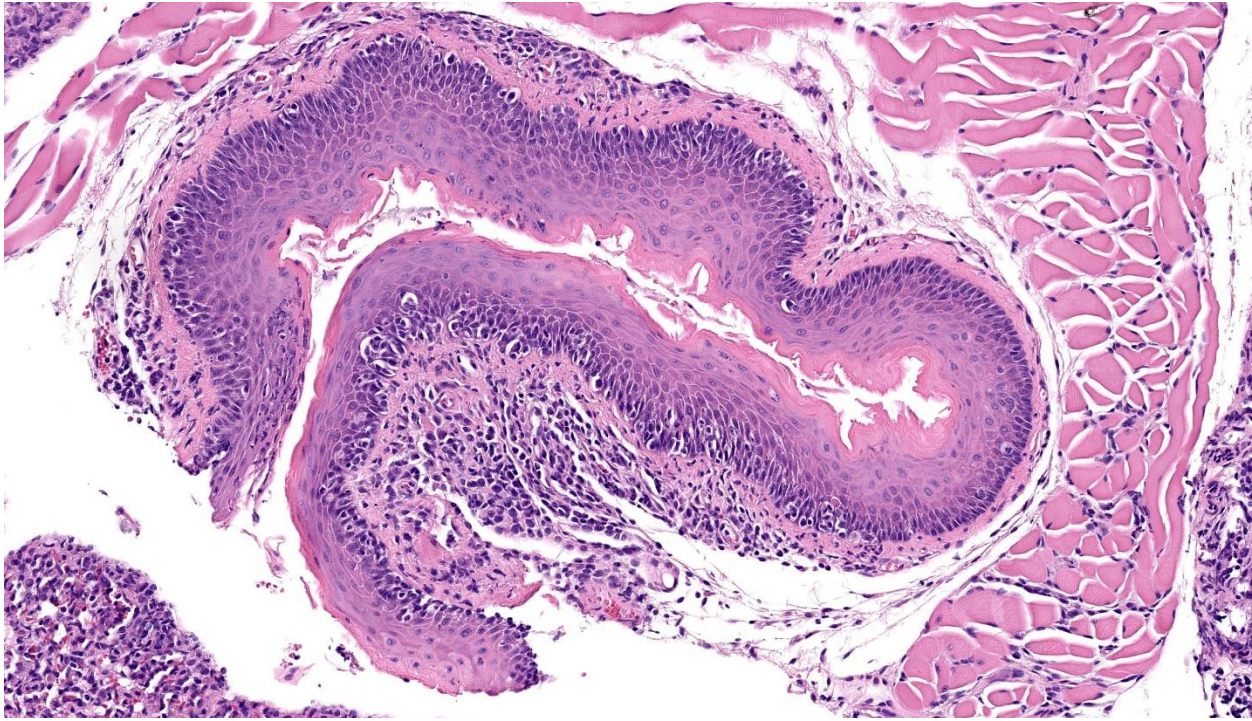


Figure 4-4. Esophagus, scid mouse. There are aggregates of lymphocytes and histiocytes within the lamina propria, which occasionally migrate into the deep layers of the mucosa. There are occasional apoptotic mucosal epithelial cells. (HE, 615X)

auto-immunity. However, in the setting of hematopoietic stem cell transplantation, the transferred immunocompetent donor T cells recognize host alloantigens as foreign, resulting in immune activation and targeting of host tissue.^{3,8} The primary effector cells are donor CD8⁺ T lymphocytes and Natural Killer cells that recognize host MHC I molecules and induce direct cytotoxicity in these cells. Alloreactive CD4⁺ T cells also contribute via recognition of MHC class II molecule differences and secretion of pro-inflammatory cytokines that induce further immune activation and tissue damage.^{3,8}

NSG mice are an extremely immunodeficient mouse model that lack natural killer cells, B lymphocytes and T lymphocytes.^{5,12} Due to the lack of a functional adaptive immune system, these mice can be engrafted with human-derived tissues including hematopoietic

stem cells, cell culture lines, and patient-derived xenografts.

Human peripheral blood mononuclear cell (hPBMC) NSG mice have become an important model in the study of GvHD, which is a major clinical problem in human hematopoietic stem cell recipients.^{4,12} hPBMC NSG mice are considered an improved model of xenogenic GvHD compared to NOD/SCID and RAG2null / IL2rynull recipients due to their earlier onset of symptoms, more pronounced weight loss, and earlier mortality.⁴ Consequently, GvHD development is expected in hPBMC NSG, resulting in a shortened lifespan of approximately 3-4 months. The disease course in this case was more rapid than experienced previously by the submitting lab.

Notably, human T cells are able to recognize murine xeno-antigens presented by murine

Table 1: Histologic Criteria for GvHD^{10,11,14}

	Criteria for acute GvHD	Criteria for chronic GvHD	This case:
Skin	Apoptosis in basal epithelium +/- vacuolar change; interface dermatitis; lymphocytic exocytosis and satellitosis	Acanthosis and hyperkeratosis; interface dermatitis; thickening and homogenization of dermal collagen +/- dermal and subcuticular sclerosis;	Lichenoid and periadnexal dermatitis with vacuolar change of basal keratinocytes
Oral cavity, oropharynx, Esophagus	Lichenoid interface inflammation; lymphocytic exocytosis; epithelial apoptosis	Lichenoid interface inflammation; lymphocytic exocytosis; epithelial apoptosis	Lichenoid interface inflammation (esophagus) with vacuolar change, epithelial apoptosis, and myofiber degeneration
Liver	Bile duct injury; lobular and portal inflammation; cholestasis	Ductopenia; progressive fibrosis; chronic cholestasis	Portal and centrilobular lymphocytic infiltration; bile duct hyperplasia and atypia
Salivary gland		Periductal lymphoplasmacytic inflammation and fibroplasia; acinar destruction and loss	Periductal lymphocytic sialadenitis with acinar loss
Intestine	Enterocyte apoptosis; crypt or basilar gland destruction; mucosal ulceration	Enterocyte apoptosis; crypt destruction, loss, distortion; mucosal ulceration; lamina propria and submucosal fibrosis	
Lung	Intrabronchiolar T cells; bronchiolar and interstitial epithelial apoptosis; perivenular cuffing; lymphocytic bronchiolitis;	Constrictive bronchiolitis obliterans; cryptogenic organizing pneumonia; chronic interstitial pneumonia	Perivascular, peribronchiolar, interstitial lymphohistiocytic inflammation with chronic atelectasis and interstitial lung injury

MHC class I and II molecules, and onset of GvHD is dependent on host expression of MHC.^{2,7} hPBMc NSG MHC I/II Double Knockout mouse models demonstrate delayed onset of xenogeneic-GvHD relative to hPBMc NSG mice, and thereby may be more suitable for immuno-oncology studies and/or long-term studies requiring human T cell engraftment.^{1,9}

The two major subdivisions of GvHD are acute versus chronic GvHD, which are defined by their clinicopathologic features not solely the time after transplantation.^{3,13} Acute

GvHD typically has rapid onset and is characterized by multiorgan lymphocytic, histiocytic, and neutrophilic inflammation with associated tissue destruction and epithelial apoptosis; the most commonly affected organs include the skin, gastrointestinal tract, and liver. In contrast, the hallmark of chronic GvHD is fibrotic/sclerotic lesions with variable leukocyte infiltration and can be observed in almost any organ.¹³ While chronic GvHD classically develops >100 days post-transplantation in patients that have previously developed acute GvHD, it can also develop de novo or simultaneously with acute

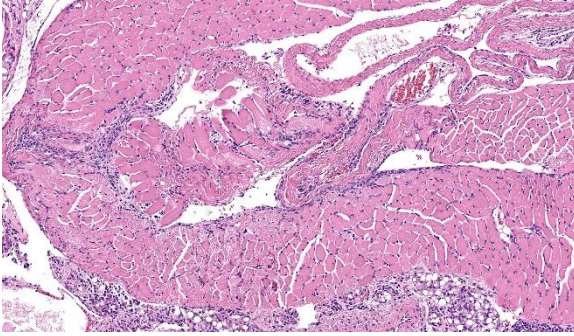


Figure 4-5. Skeletal muscle, scid mouse. Low to moderate number of lymphocyte and histiocytes infiltrate beneath the epimysium and within the perimysium of skeletal muscle. (HE, 197X)

GvHD.^{3,6,13} An abbreviated summary of the histologic criteria for acute and chronic GvHD and a comparison to features supportive of a diagnosis of xenogeneic GvHD in this case are included in Table 1.

Onset and progression of GvHD in this ‘humanized’ mouse was likely further accelerated and exacerbated by the additional injection of non-matched, human-derived tumor cells. Failure of tumor engraftment in these mice is also consistent with a hu-PBMC-derived immune response against the tumor.⁹ Given that the entire cohort of mice appeared affected, it is also possible these hPBMCs were unusually reactive resulting in accelerated onset of GvHD.

Expected lung changes in GvHD are characterized by intrabronchiolar T cells, apoptosis, and perivenulitis, which can progress acutely to respiratory distress and death, or to constrictive bronchiolitis obliterans (CBO) in chronic GvHD.^{11,14} Fibrosis was not prominent in these lung sections, which is attributed to the relatively short course of disease. Lung changes are more extensive than in similar cases here, and may suggest a role for opportunistic infection as a contributor to mortality in this cohort (e.g., *Chlamydia* spp. infection). *Mycoplasma pulmonis* and *Filo-*

bacterium rodentium are excluded from rodent areas at this site. As bacteria were not identified with Gram stain and the clinical concern resolved after that cohort, further diagnostics were not pursued.

Contributing Institution:

Johns Hopkins University, School of Medicine

Department of Molecular and Comparative Pathobiology

<https://mcp.bs.jhmi.edu/>

JPC Diagnosis:

1. Lung: Pneumonia, interstitial and lymphohistiocytic, subacute, diffuse, marked, with perivascular and peribronchiolar lymphoid proliferation.
2. Esophagus: Esophagitis, interface and lymphocytic, subacute, multifocal, moderate.
3. Skeletal muscle: Myositis, lymphocytic, subacute, multifocal, moderate.
4. Thyroid gland: Thyroiditis, lymphocytic, subacute, multifocal, mild.
5. Adipose tissue: Steatitis, lymphocytic, subacute, multifocal, mild.

JPC Comment:

The final case of this conference provided a healthy challenge for participants, with the knowledge of hematopoietic stem cell involvement in this humanized mouse being essential for understanding the underlying pathogenesis that the contributor nicely summarizes. We opted for multiple morphologic diagnoses to capture the distribution of inflammatory cells, though the underlying changes were similar across the lung, esophagus, skeletal muscle, thyroid, and adjacent adipose tissue. We did note a very mild acidophilic macrophage pneumonia in this mouse, though this is a non-specific finding and

likely follows from the marked inflammation of the lung.

The contributor IHC results help to describe the distribution of inflammatory cells in this case. With the assistance of Dr. Radaelli, we further characterized these cells with the aid of a mouse-specific CD86 (B7; marker of antigen presenting cell), CD4/CD8 (T-cell markers), and CD79 (B-cell). CD86-positive cells were widely distributed in tissue while B-cells were sparse in the lung with none in esophagus or muscle. CD4+ T-helper cells were present in moderate numbers in the lung, muscle, and esophagus while CD8+ cytotoxic T-cells were notable in the lung, esophagus, and the thyroid with the latter not being as obvious on the H&E section. One limitation is that we did not have a human macrophage marker available (e.g. CD45) to fully demonstrate the xenogeneic attack inherent in this case however.

Finally, Dr. Radaelli discussed humanized mice as well as several of the undesired consequences of this exploratory model during his pre-conference lecture which we abridge here.⁹ Humanized mice are interspecies chimeras that offer a potential avenue to explore tumor oncogenic signatures (biomarkers), test therapeutic interventions, and assess relative toxicity therein through a stable line that supports continued/stable tumor growth. Because these mice are severely immunosuppressed and bathed in a veritable shower of cytokines to enhance human hematopoietic stem cell line proliferation, there is also the possibility of myeloid cell hyperactivation,¹⁵ excessive lymphoproliferation, and even oncogenic activation of latent viruses (e.g. Epstein-Barr virus) in human tissue grafts.¹⁶ Opportunistic infection, as seen in Case 1 of this conference, is yet another consideration. While the

potential benefits of this model are significant, pathologists also play an important role in advocating for the welfare of these mice and identifying issues or limitations of a given mouse type.¹⁷

References:

1. Brehm MA, Kenney LL, Wiles MV, et al. Lack of acute xenogeneic graft-versus-host disease, but retention of T-cell function following engraftment of human peripheral blood mononuclear cells in NSG mice deficient in MHC class I and II expression. *FASEB J.* 2019;33(3):3137-3151.
2. Ehx G, Somja J, Warnatz HJ, et al. Xenogeneic Graft-Versus-Host Disease in Humanized NSG and NSG-HLA-A2/HHD Mice. *Front Immunol.* 2018;9:1943.
3. Ghimire S, Weber D, Mavin E, Wang XN, Dickinson AM, Holler E. Pathophysiology of GvHD and Other HSCT-Related Major Complications. *Front Immunol.* 2017;8:79.
4. Ito R, Katano I, Kawai K, et al. Highly sensitive model for xenogenic GVHD using severe immunodeficient NOG mice. *Transplantation.* 2009;87(11):1654-1658.
5. The Jackson Laboratory. Strain 005557 NOD.Cg-Prkdcscid Il2rgtm1Wjl/SzJ. Accessed June 28, 2023. <https://www.jax.org/strain/005557>.
6. Jagasia MH, Greinix HT, Arora M, et al. National Institutes of Health Consensus Development Project on Criteria for Clinical Trials in Chronic Graft-versus-Host Disease: I. The 2014 Diagnosis and Staging Working Group report. *Biol Blood Marrow Transplant.* 2015;21(3):389-401.e1.
7. King MA, Covassin L, Brehm MA, et al. Human peripheral blood leucocyte non-obese diabetic-severe combined immunodeficiency interleukin-2 receptor gamma

- chain gene mouse model of xenogeneic graft-versus-host-like disease and the role of host major histocompatibility complex. *Clin Exp Immunol*. 2009;157(1):104-118.
8. Kumar V, Abbas AK, Aster JC. Diseases of the immune system. *In: Robbins and Cotran Pathologic Basis of Disease*, 10th ed. Philadelphia, PA, Elsevier Saunders; 2021.
 9. Radaelli E, Hermans E, Omodho L, et al. Spontaneous Post-Transplant Disorders in NOD.Cg-Prkdcscid Il2rgtm1Sug/JicTac (NOG) Mice Engrafted with Patient-Derived Metastatic Melanomas. *PLoS One*. 2015;10(5):e0124974.
 10. Salomao M, Dorritie K, Mapara MY, Sepulveda A. Histopathology of Graft-vs-Host Disease of Gastrointestinal Tract and Liver: An Update. *Am J Clin Pathol*. 2016;145(5):591-603.
 11. Shulman HM, Cardona DM, Greenson JK, et al. NIH Consensus development project on criteria for clinical trials in chronic graft-versus-host disease: II. The 2014 Pathology Working Group Report. *Biol Blood Marrow Transplant*. 2015;21(4):589-603.
 12. Shultz LD, Brehm MA, Garcia-Martinez JV, Greiner DL. Humanized mice for immune system investigation: progress, promise and challenges. *Nat Rev Immunol*. 2012;12(11):786-798.
 13. Vigorito AC, Campregher PV, Storer BE, et al. Evaluation of NIH consensus criteria for classification of late acute and chronic GVHD. *Blood*. 2009;114(3):702-708.
 14. Xu L, Drachenberg C, Tavora F, Burke A. Histologic findings in lung biopsies in patients with suspected graft-versus-host disease. *Hum Pathol*. 2013;44(7):1233-1240.
 15. Tarrant JC, Binder ZA, Bugatti M, et al. Pathology of macrophage activation syndrome in humanized NSGS mice. *Res Vet Sci*. 2021 Jan;134:137-146.
 16. Tillman H, Vogel P, Rogers T, Akers W, Rehg JE. Spectrum of Posttransplant Lymphoproliferations in NSG Mice and Their Association With EBV Infection After Engraftment of Pediatric Solid Tumors. *Vet Pathol*. 2020 May;57(3):445-456.
 17. Willis E, Verrelle J, Banerjee E, et al. Humanization with CD34-positive hematopoietic stem cells in NOG-EXL mice results in improved long-term survival and less severe myeloid cell hyperactivation phenotype relative to NSG-SGM3 mice. *Vet Pathol*. 2024 Jul;61(4):664-674.